Jpn J Radiol (2013) 31:105–114
DOI 10.1007/s11604-012-0156-6

ORIGINAL ARTICLE

Dynamic characteristics of MR diffusion-weighted imaging in a rabbit liver VX-2 tumor model

You-Hong Yuan · En-Hua Xiao · Zhong He · Ke Jin · Cong Ma · Jun Xiang · Jian-Hua Xiao · Wei-Jian Chen

Received: 16 February 2012 / Accepted: 23 October 2012 / Published online: 13 December 2012

Abstract
Purpose To investigate prospectively dynamic characteristics of the apparent diffusion coefficient (ADC) on MR diffusion-weighted imaging (DWI) in a rabbit VX-2 tumor model.
Materials and methods Forty New Zealand rabbits were included in the study, and 47 rabbit VX-2 tumor models were developed by direct and intrahepatic implantation after opening the abdominal cavities. DWI was carried out periodically and respectively on days 7, 14 and 21 after implantation. The VX-2 tumor samples were studied by pathology. The distinction of VX-2 tumors on DWI was assessed by their ADC values by analysis of variance (ANOVA) using SPSS12.0 software.
Results The ADC values (mean ± SD) × 10^{-3} mm^2/s of 47 VX-2 tumors in the peripheral and central areas were 2.18 ± 0.29, 1.96 ± 0.33, 1.80 ± 0.35, 2.20 ± 0.29, 2.05 ± 0.30 and 1.96 ± 0.48, respectively, on days 7, 14 and 21 after implantation. ADC values of 47 VX-2 tumors in the area of the tumor periphery, center and normal parenchyma were higher when the *b*-value was 100 s/mm^2 than those when the *b*-value was 300 s/mm^2 ($F = 17.964$, $p < 0.001$; $F = 13.986$, $p < 0.001$; $F = 128.681$, $p < 0.001$). ADC values in the area of normal liver parenchyma were higher than those in the area of the VX-2 tumor periphery and center when the *b*-value was 100 or 300 s/mm^2. ADCs of viable tumor cells in VX-2 tumors were lower on DWI than those in the area of normal liver parenchyma around the tumor, and ADCs of dead tumor cells in VX-2 tumors were unequal, including high, equal and low values, but they were higher than in the area of normal liver parenchyma around tumors after dead tumor cells had been liquefied or had become cystic.
Conclusion ADC is correlated with the tumor histology and degree of malignancy, and DWI has potential value for dynamically monitoring tumors and evaluating the degree of malignancy and therapeutic effect.

Keywords Liver · VX-2 tumor · Diffusion-weighted imaging · Apparent diffusion coefficient (ADC) · Rabbit

Y.-H. Yuan · E.-H. Xiao (✉) · Z. He · C. Ma · J. Xiang
Department of Radiology, The Second Xiang-Ya Hospital, Central South University, Changsha 410012, Hunan, China
e-mail: heyuanyouhong@yahoo.com.cn; yyh82278441@163.com

K. Jin · J. Xiang · W.-J. Chen
Department of Pathology, Hunan Province Children's Hospital, Changsha 410005, Hunan, China

J. Xiang · J.-H. Xiao
Department of Epidemiology, Center for Disease Control of Hunan Province, Changsha 410005, Hunan, China

Introduction

A variety of imaging modalities, including ultrasound (US), computed tomography (CT), magnetic resonance imaging (MRI), nuclear medicine and angiography, is currently used in diagnosing and evaluating hepatocellular carcinoma (HCC) [1–5]. Further technological advancement will undoubtedly have a major impact on liver tumor imaging. Increased speed of data acquisition and consequently shorter scan times in MRI show further improvement in resolution by further reducing motion artifacts [4–8]. Advances in MR technology, including hardware and pulse sequence implementation, allow acquisition times to be reduced to the time frame of one breath-hold, providing multiphasic dynamic MRI. Functional MRI including diffusion-weighted imaging (DWI) has been investigated for

the clinical utility of detection and characterization of HCC [6–17].

DWI is an imaging technique that provides tissue contrast by the measurement of diffusion properties of water molecules within tissues. Diffusion is expressed in an apparent diffusion coefficient (ADC), which reflects the diffusion properties unique to each type of tissue. With assessment of ADC values, DWI has proved to be helpful in the characterization of focal liver lesions [10–17].

As reported in many clinical data, the ADCs of different liver lesions have different characteristics, and their quantitative measurement can provide a potential and promising functional imaging tool for predicting the histological grade and early recurrence before treatment. ADCs (mean ± SD × 10^{-3} mm^{-2}/s) were significantly lower in HCC (1.31 ± 0.28) and liver metastasis (1.11 ± 0.22) and were significantly higher in hemangioma (1.84 ± 0.37) and cyst (2.61 ± 0.45) than in the surrounding hepatic tissues [11]. Benign lesions had higher ADC values than malignant lesions, but those of solid benign lesions [focal nodular hyperplasia (FNH) and adenomas] were similar to those of solid malignant lesions (metastases and HCCs) [12]. These results are the same as those reported by Nishie et al. [4]. The histopathological differentiation of HCC shows an inverse correlation with the ADC value [13]. The pre-chemoembolization HCC ADC was 1.36 ± 0.25, while the change in ADC post-chemoembolization was 0.377 ± 0.33. Pre-treatment ADC values as well as changes in ADC values after treatment may provide useful information for predicting survival for patients with unresectable hepatocellular carcinoma [14, 15]. The ADC values of necrotic tissues with lipiodol, necrotic tissues without lipiodol, viable tumors and normal liver tissues were 1.905 ± 0.487, 0.726 ± 0.116, 1.449 ± 0.054 and 1.777 ± 0.094, respectively. The ADC values of 3.0-T MR DWI can be used to distinguish the viable residue or recurrent tumor tissues and necrotic tissues in HCC after TACE [14]. There was a significant differences between the ADC of viable tissue and that of necrotic tumor tissue (1.33 ± 0.41 vs. 2.04 ± 0.38). There was a moderately significant correlation between ADC and the pathological finding of the percentage of necrosis and a highly significant correlation between the subtraction image and the pathological percentage of necrosis [15, 16].

Therefore, DWI has been applied for detecting and characterizing tumors. In addition, this technique is so quick to perform that it can be incorporated into a standard clinical protocol. Although several DWI studies have focused on the ADC value, few reports have examined the relationship between the ADC values and the histological characteristics in a rabbit VX-2 tumor model dynamically and image-pathologically. Our hypothesis is that the tumor ADC value is closely correlated with the pathological grading of the cancer and the degree of liquefaction and necrosis, so that the ADC of the tumor can be used to indicate the histological characteristics, monitor tumor growth and evaluate the degree of malignancy and therapeutic effect. The purpose of our prospective study was to evaluate the relationship between the histopathological differentiation and ADC measurement on DWI in a rabbit VX-2 tumor model as a part of our research series on DWI [18–21]. However, these studies did not use a rabbit VX-2 tumor model on days 7, 14 and 21 after transplantation or compare the ADC distinction in the area of the VX-2 tumor periphery, center or normal liver parenchyma around the tumor.

Materials and methods

Animals and establishment of the VX-2 tumor model

Animal studies were carried out under the supervision of a veterinarian according to *The Guidelines of the Ministry of Public Health of China for the Use of Laboratory Animals*. All animals were provided by the Laboratory Animal Center of the Second Xiangya Hospital or Hunan Province People's Hospital, and all protocols were approved by the Animal Use and Care Committee and Medical Ethics Committee of the Second Xiangya Hospital.

Forty New Zealand rabbits were included in the study. Twenty-two were male rabbits and 18 were female, weighting from 1.7 to 2.5 kg and aged from 5 to 6 months. All New Zealand white rabbits were healthy. After animals had been anesthetized by injecting 3 % soluble pentobarbitone into an auriborder vein at a dose of 1 ml/kg, VX-2 strains were implanted directly and intrahepatically after opening the abdominal cavity. In the experiment, 25 New Zealand white rabbits in the experiment were implanted in one lobe, while 15 were implanted in two lobes. The VX-2 tumor strain of rabbit was provided by the Fourth Military Medical University.

Magnetic resonance imaging protocol [17–19]

After animals had been anesthetized by injecting 3 % soluble pentobarbitone into an auriborder vein at a dose of 1 ml/kg or at different doses based on different animal statuses to make sure that the breathing of animals was slow and stable, DWI (axial) was carried out respectively and periodically on a 1.5-T Signal Twinspeed MR scanner (General Electron Medical Systems, USA) using a small-diameter cylindrical brain radiofrequency coil on days 7, 14 and 21 after implantation. The DWI scanning parameters included a spin echo echoplanar imaging (SE-EPI) series, *b*-value 100 and 300 s/mm^2, repetition time (TR)

6,000 ms, echo time (TE) 45 ms, 20 cm × 15 cm field of view (FOV), 8NEX, 2-mm-thick layer, 0.5 mm Space, 128 × 128 matrix, etc.

ADC values and signal values in the area of the VX-2 tumor periphery, VX-2 tumor center and normal liver parenchyma, around the tumor (Fig. 1) were obtained using Function software in the GE Workstation. Three different regions of interest (ROIs) (50 mm^2 in each area) were chosen in the area of normal liver parenchyma (Fig. 1, area D), and we measured their ADC values and signal values. The average value was considered as the ADC value or the signal value of normal liver parenchyma around the tumor. The thickness of area A and B in Fig. 1 was two-fifths of the diameter of the VX-2 tumor, respectively. By the same methods, the average value of three different ROIs, ADC values or signal values in area B was considered as the ADC value or the signal value of the VX-2 tumor periphery area, and the ADC value or signal value in area A represented the VX-2 tumor center area. All measurements were finished cooperatively by two senior attending physicians or associate professors.

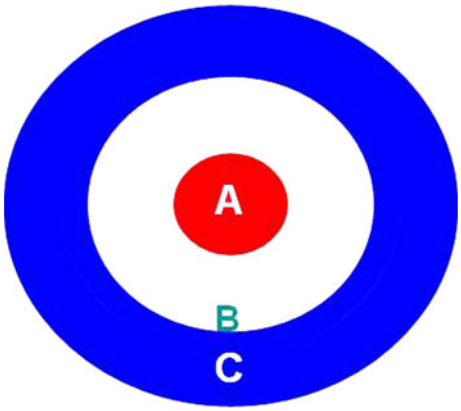

Fig. 1 *A*, *B* and *C* areas representing respectively the area of the VX-2 tumor center, periphery and normal liver parenchyma area around the tumor when the ADC and signal values were measured on DWI and samples were investigated pathologically

Pathology protocol

Twelve VX-2 tumor samples were analyzed pathologically. Of these, ten samples were obtained on day 21 after implantation and one on day 7 after implantation, while another was obtained on day 14. Then we cut them open and made samples layer by layer (Fig. 1). We used mouse anti-rabbit antibody manufactured by Millipore.

Statistical analysis

Based on the apparent diffusion coefficient (ADC) value of the regions of interest (ROIs), images were evaluated quantitatively, including the distinction among different area groups, different time groups and different *b*-value groups. The statistical significance was calculated by analysis of variance (ANOVA) using SPSS software (version 12.0; SPSS, Tokyo, Japan).

Results

Image manifestations of hepatic VX-2 tumor

ADC values and signal values of 47 VX-2 tumors are shown in Table 1 and Figs. 2, 3, and 4.

The distinction of ADC in the area of the VX-2 tumor periphery, VX-2 tumor center or normal liver parenchyma around the tumor between different b-value groups was significant ($F = 17.964, p < 0.001$; $F = 13.986, p < 0.001$; $F = 128.681$, $p < 0.001$) when the *b*-value was 100 or 300 s/mm^2. Signals in 47 cases in the area of the VX-2 tumor periphery, VX-2 tumor center and normal liver parenchyma around the tumor were higher when the *b*-value was 100 s/mm^2 than when the *b*-value was 300 s/mm^2, and the distinction in 47 cases between different *b*-value groups was significant ($Z = -17.737$, $p = 0.000$).

The distinctions of the ADC in the area of the VX-2 tumor periphery or tumor center on days 7, 14 and 21 after implantation were respectively significant ($b = 100$ s/mm^2, $F = 48.211$, $p < 0.001$; $b = 300$ s/mm^2, $F = 20.955$, $p < 0.001$). The distinction of ADC in the area of normal

Table 1 ADC values of tumor and normal parenchyma (mean ± SD) × 10^{-3} mm^2/s

	VX-2 tumor periphery area		VX-2 tumor center area		Normal hepatic parenchyma	
	$b = 100$	$b = 300$	$b = 100$	$b = 300$	$b = 100$	$b = 300$
A	2.18 ± 0.29	2.10 ± 0.27	2.20 ± 0.29	2.12 ± 0.29	2.82 ± 0.36	2.27 ± 0.29
B	1.96 ± 0.33	1.78 ± 0.37	2.05 ± 0.30	1.90 ± 0.44	2.61 ± 0.40	2.22 ± 0.39
C	1.80 ± 0.35	1.60 ± 0.27	1.96 ± 0.48	1.71 ± 0.33	2.75 ± 0.43	2.19 ± 0.34
Total	1.98 ± 0.36	1.83 ± 0.37	2.07 ± 0.38	1.98 ± 0.38	2.73 ± 0.41	2.23 ± 0.34

A, day 7 after implantation; B, day 14 after implantation; C, day 21 after implantation

parenchyma around the tumor between day 7 and 14 was significant (Tukey HSD, $p < 0.05$) but that between day 7 and 21 or between day 14 and 21 was insignificant (Tukey HSD, $p > 0.05$). From day 7 to 14 or day 21 when the *b*-value was 100 s/mm^2, signal values in the area of the VX-2 tumor periphery or normal liver parenchyma around the tumor increased and the signal distinction among them was significant ($x[2] = 8.340$, $p = 0.015$; $x[2] = 20.723$, $p < 0.001$), but signals in the area of the VX-2 tumor center became large, and the signal distinction among them was insignificant ($x[2] = 3.106$, $p = 0.212$).

When the *b*-value was 100 or 300 s/mm^2, the ADC distinction among the VX-2 tumor periphery area, center area and normal liver parenchyma around the tumor was respectively significant ($b = 100$ s/mm^2, $F = 176.586$, $p < 0.001$; $b = 300$ s/mm^2; $F = 55.089$, $p < 0.001$). When the *b*-value was 100 s/mm^2, signals in the area of the VX-2 tumor periphery, VX-2 tumor center or normal liver parenchyma around the tumor were higher than that when the b-value was 300 s/mm^2 ($p < 0.001$).

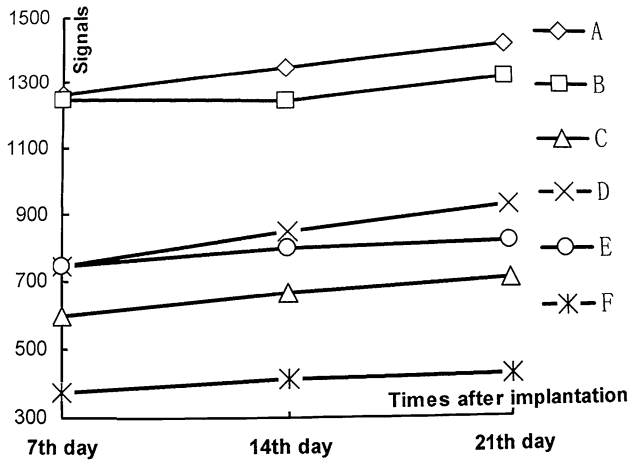

Fig. 2 Dynamic characteristics of signal values on DWI when the area and *b*-value were different after implantation. *A* Signal of the VX-2 tumor periphery area when the *b*-value was 100 s/mm^2; *B* signal of the VX-2 tumor center area when the *b*-value was 100 s/mm^2; *C* signal of the normal liver parenchyma area around the tumor when the *b*-value was 100 s/mm^2; *D* signal of the VX-2 tumor periphery area when the *b*-value was 300 s/mm^2; *E* signal of the VX-2 tumor center area when the *b*-value was 300 s/mm^2; *F* signal of the normal liver parenchyma area around the tumor when the *b*-value was 300 s/mm^2

Manifestations of VX-2 tumor pathology

On day 7 and 14 after implantation, intrahepatic VX-2 tumors were pale with no envelope or identifiable margin, and no lumps were detected in the hepatic parenchyma near the VX-2 tumor, but there were residua of gelatin sponge in or around the VX-2 tumor.

Under the microscope, the inequality of size, round or ellipse tumor nests could be observed in VX-2 tumors, but there were more blood capillaries and relatively few intercellular substances or connective tissues. Calcification focus and residuum of gelatin sponge could be observed in some cases. Most center areas of the VX-2 tumor were necrotic, but there were a few necroses in the area of the tumor periphery (Fig. 5). Necrotic cells showed disrupted cell membranes and fragmented cell nuclei, or they dissolved and disappeared (Figs. 5, 6, 7). There were relatively few intercellular substances in tumors, so the karyoplasmic ratio was disturbed. The size of the cellular

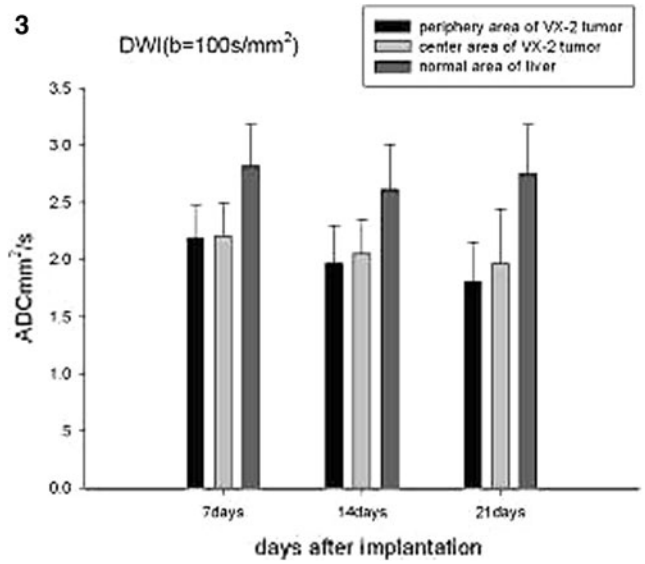

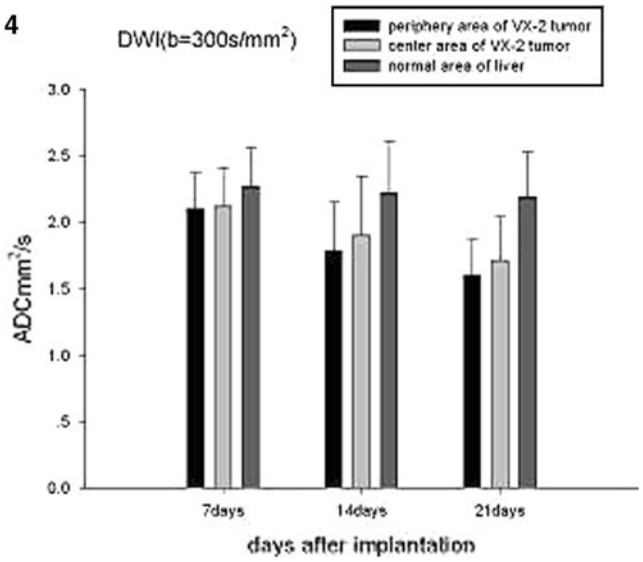

Figs. 3–4 Dynamic characteristics of ADC values of different areas on DWI after implantation. **Fig. 3** The *b*-value was 100 s/ mm^2; **Fig. 4** The *b*-value was 300 s/mm^2

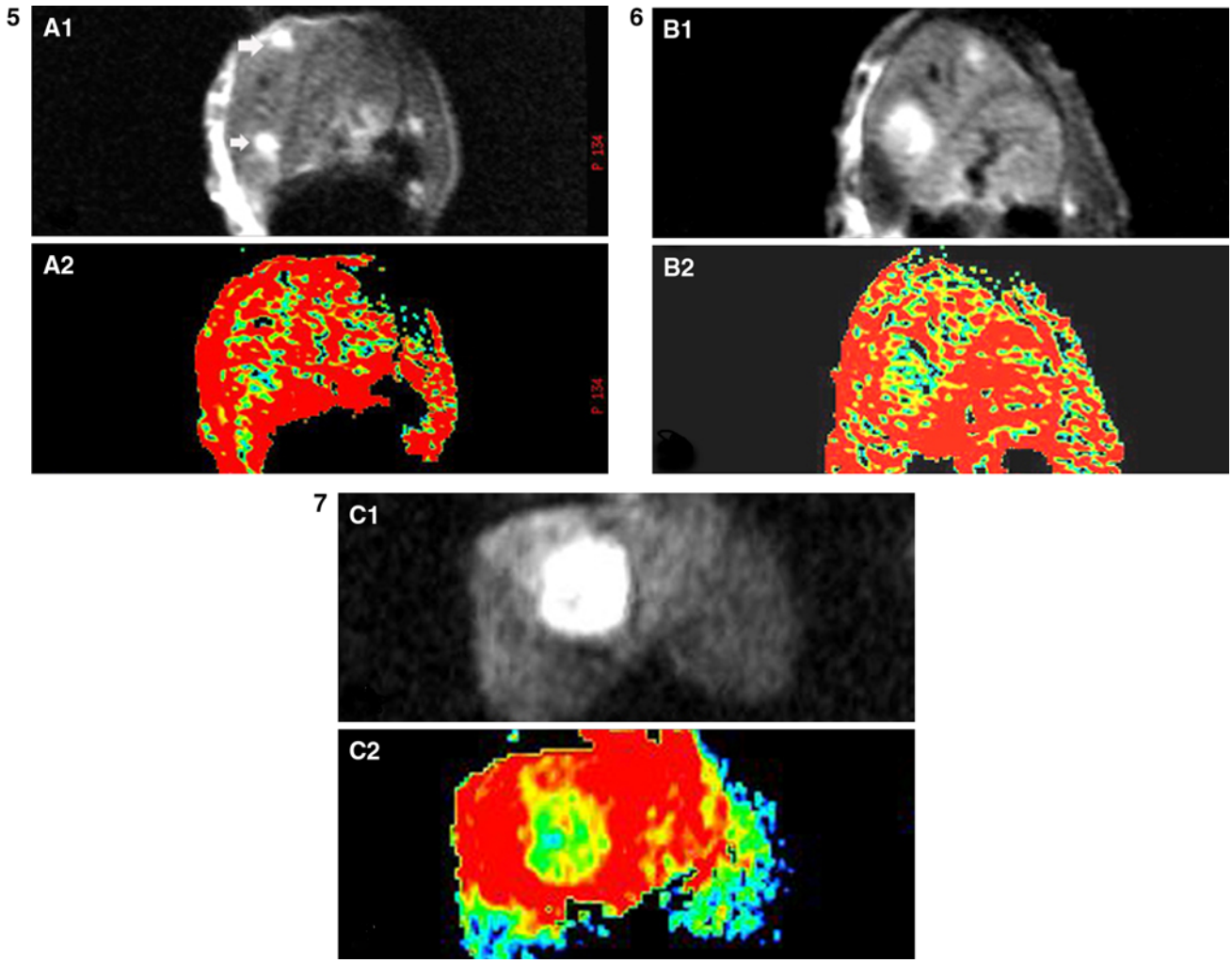

Figs. 5–7 Image manifestations of hepatic VX-2 tumor on DWI and ADC map. **Fig. 5** *A1* High signal and distinct margin of VX-2 tumor on DWI; *A2* equal signal on the ADC map when the *b*-value was 100 s/mm^2 on day 7 after implantation. **Fig. 6** *B1* High signal and distinct margin of VX-2 tumor on DWI and *B2* low signal on the ADC map when the *b*-value was 100 s/mm^2 on day 14 after implantation (note: the tumor in the posterior area of the right hepatic lobe grew significantly, while the tumor in the anterior area of the right hepatic lobe did not, so its implantation is unsuccessful). **Fig. 7** *C1* High signal and distinct margin of the VX-2 tumor on DWI and *C2* low signal and distinct margin on the ADC map when the *b*-value was 300 s/mm^2 on day 21 after implantation

nucleus was uneven and the number of cellular nuclei was unequal in cells. Most of the cellular nucleus was dyed deeply, and some had obviously abnormal caryocinesia.

Discussion

DWI, a functional MRI technique, detects MR signal changes in tissues due to water proton motion, known as Brownian motion, which varies based upon the degree of cell membrane integrity [3–5]. The intact membranes of viable tumor cells restrict water diffusion, whereas necrotic tumor cells with disrupted cell membranes exhibit increased water diffusion. This mobility of water is quantified by a constant known as the ADC. Previous preclinical and clinical studies [4–17], including ours and others [18–21], have shown that tumor necrosis is associated with an increase in ADC value, thereby allowing differentiation between viable and necrotic portions of tumors. The degree of malignancy is closely connected with cellularity [22–25] and a remarkable correlation between ADC values and tumor necrosis [26].

From our experience, ADC values of 47 cases in the area of the VX-2 tumor periphery and tumor center were lower than those in the area of normal liver parenchyma around the tumor ($p < 0.01$). ADCs of 47 cases in the area of the VX-2 tumor periphery decreased gradually after implantation, and there were many tumor nests containing a great quantity of viable and intensive tumor cells in which cell nucleus heteromorphism was high, and there were few dead or apoptotic cells in this area. Because the diffusion of tumor cells was obviously limited, the ADC in

the area of the VX-2 tumor periphery decreased significantly and was smaller than those in the area of normal parenchyma around the tumor. After implantation, the ADC of tumors decreased because tumors grew increasingly quickly along with VX-2 tumor cells overcoming autoimmunity, and re-establishment of VX-2 tumor vessels increased gradually so that the limitation of water molecular motion in the tumor increased greatly. From day 7 after implantation to day 14 or 21 after implantation, ADCs of VX-2 tumors in the area of the tumor center fell gradually, but the degree of the decrease was smaller than in the ADCs of VX-2 tumors in the tumor periphery area, especially from day 14 to 21 after implantation. The ADC of low or high signal areas in the area of the tumor center was higher than that in other areas, including equal signal areas (relative to the signal of the tumor periphery), the area of the tumor center, the area of the tumor periphery or the area of normal liver parenchyma around the tumor, and the low signal areas above were coagulation necroses, while the high signal areas above were liquid because of coagulation necrosis having been liquefied or become cystic (Figs. 8, 9, 10, 11).

From day 7 after implantation to day 14 or 21 after implantation, the ADC in the area of normal liver parenchyma around the tumor decreased and the signals increased ($p < 0.01$), but the degree of the ADC or the

Fig. 8 Sample on day 21 after implantation

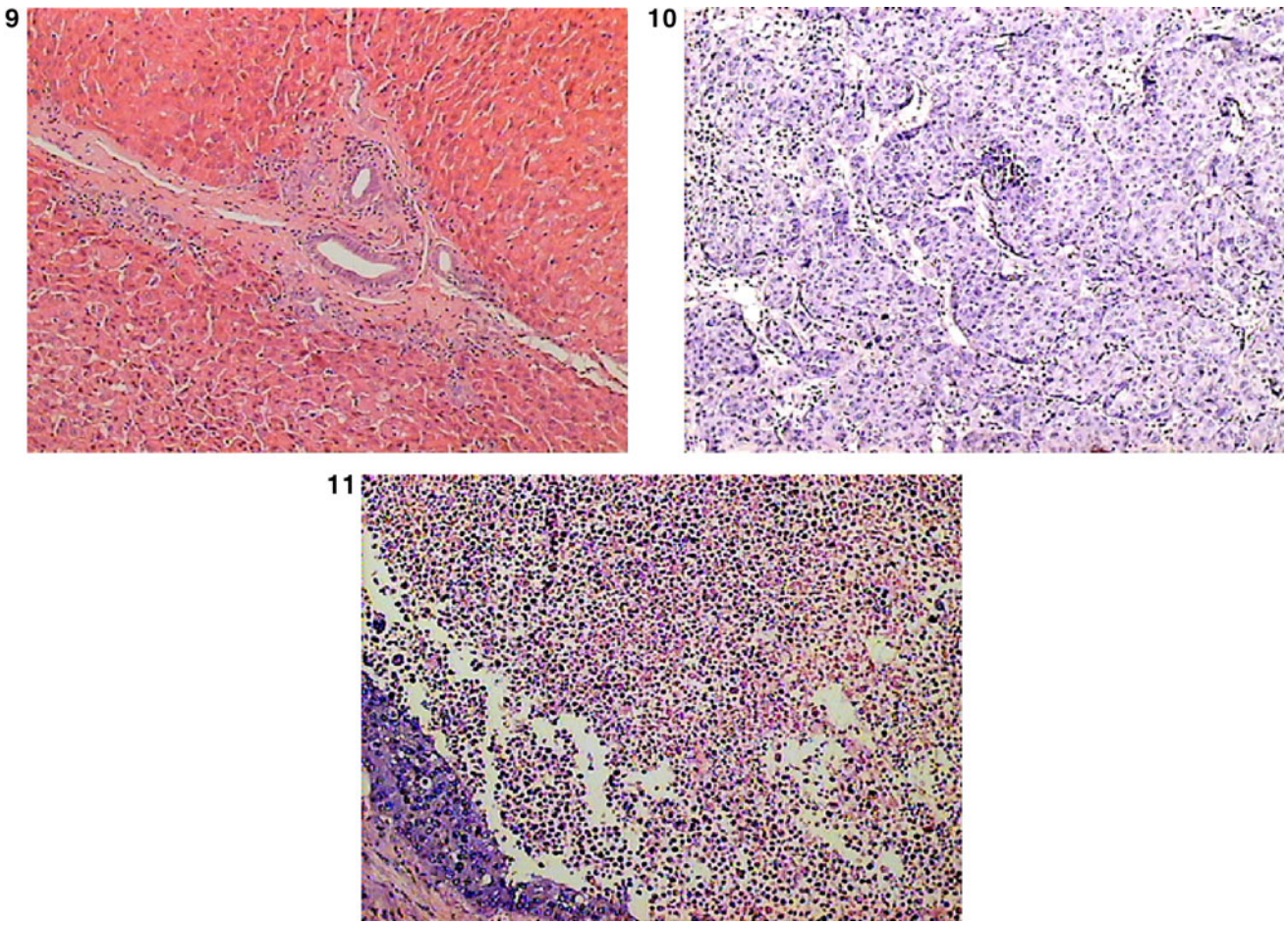

Figs. 9–11 Normal liver parenchyma, tumor outer layer and the tumor center of the VX-2 tumor under a ×100 microscope

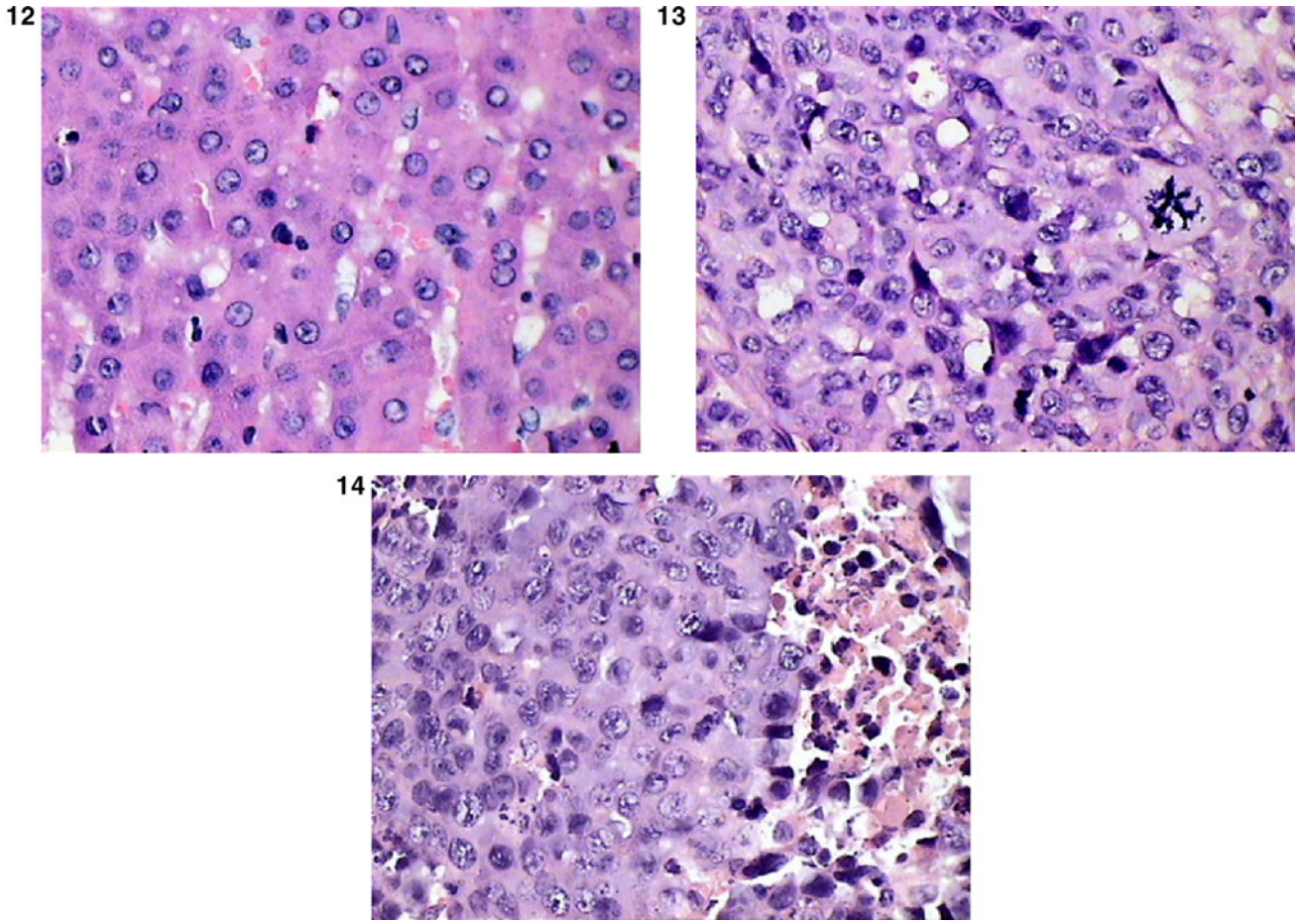

Figs. 12–14 Normal liver parenchyma, tumor outer layer and the tumor center of VX-2 tumor under a ×400 microscope

signal change was respectively smaller than that in the area of the VX-2 tumor periphery or tumor center. Confirmed by pathology, cells in the area of the liver parenchyma were normal, and the cellular nuclei were mostly equal in size; there was no caryocinesia, but there were some inflammatory cells in the blood vessels and some edema cells that contained ballooning degeneration; dead cells were not observed in the area of normal parenchyma around the tumor. On the ADC map, most of the VX-2 tumors manifested equal signals and obscure borders on day 7 after implantation, with high or low signals, and they still showed obscure borders on day 14 and low signals and distinct borders on day 21 (Figs. 12, 13, 14).

The VX-2 tumor is a solid tumor, and the lump mainly consists of tumor nests and other cells so that its water molecular diffusion motion is obviously restricted. The signals are significantly high. When coagulation necrosis took place in the tumor because the blood provision was insufficient, the cellular membrane broke, and the limitation of the water molecular diffusion motion in the tumor decreased greatly so that the signals decreased while the ADC increased. After the coagulation necrosis had liquefied or become cystic, cell lysis and leakier cell membranes could no longer compartmentalize water molecules and allowed free diffusion to take place so that the ADC values increased greatly [15–19]. However, the signals of the above were higher than those of coagulation necrosis, even of the viable tumor area or of the normal parenchyma area. This can be explained by the presence of greater amounts of extracellular water molecules within the necrotic region, which is a kind of long T2-value contribution, and the *b*-value is 100 or 300 s/mm2. Small *b*-values are significantly affected by "shine through" [20, 21] (Figs. 15, 16, 17, 18).

Wang et al. [22], Youn et al. [23], Deng et al. [24, 25] and Vossen et al. [26] demonstrated that the constitution ADC values were relatively large and unstable when the *b*-value was small or the distinction between two *b*-values was small on diffusion-weighted imaging scanning because, at this time, the ADC reflected microcirculation blood flow of the regional constitution at different degrees, and the diagnostic value would be decreased. ADC values of 47 cases in the area of the VX-2 tumor periphery, tumor center or normal liver parenchyma around the tumor were

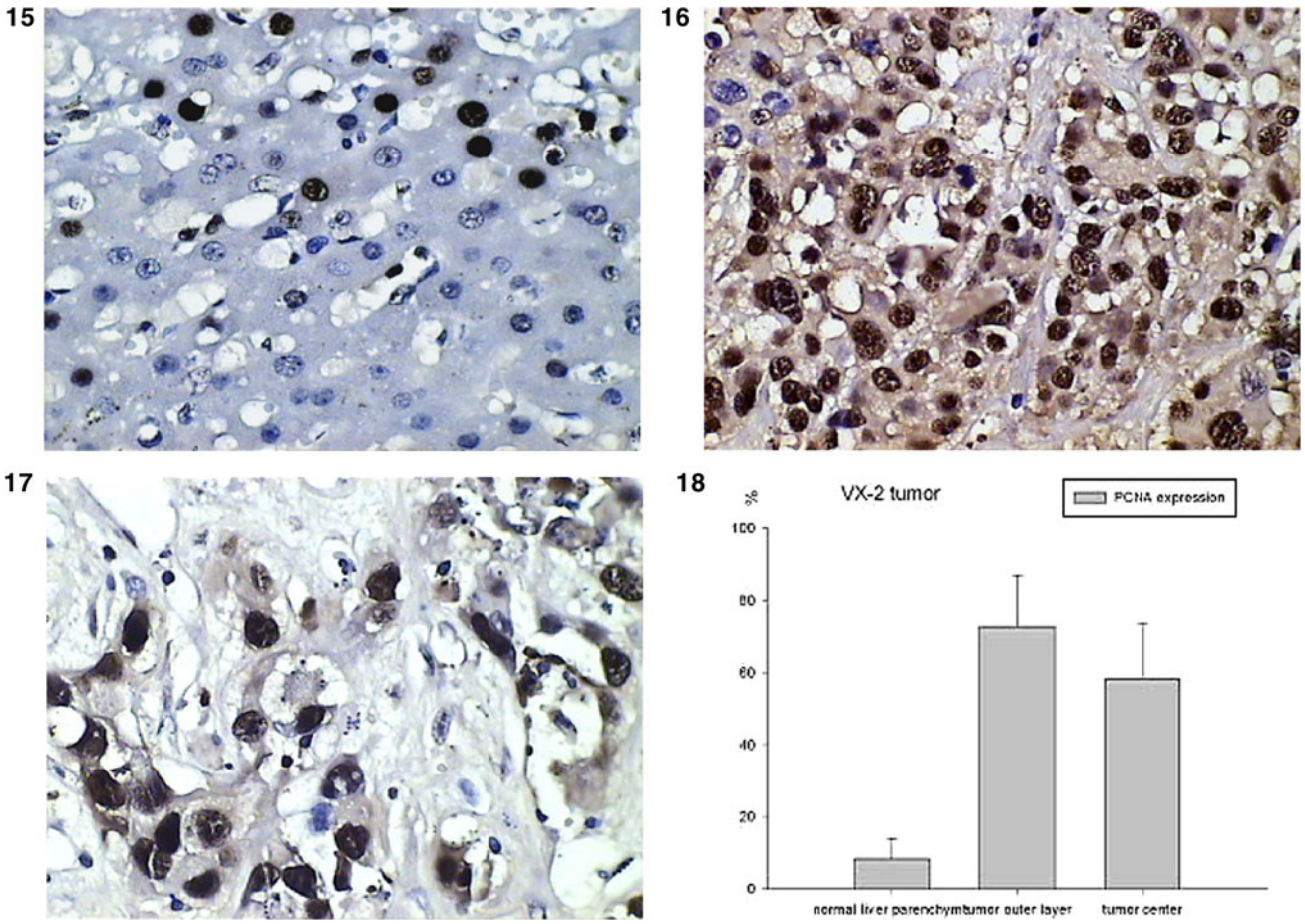

Figs. 15–18 Expression of PCNA for normal liver parenchyma, the outer tumor layer and the tumor center of the VX-2 tumor under a ×400 microscope

higher when the *b*-value was 100 s/mm^2 than when the *b*-value was 300 s/mm^2, and their signal also reduced significantly when the *b*-value was 300 s/mm^2. The ADC in the area of normal liver parenchyma around the tumor was higher than in the area of the VX-2 tumor periphery or VX-2 tumor center when the *b*-value was 100 or 300 s/mm^2. Relative to the *b*-value of 100 s/mm^2, water molecules will experience a large gradient field when the *b*-value is 300 s/mm^2. Also the signals of constitution are reduced more and ADC is affected less by the microcirculation so that, at this time, the ADC of constitution gets closer to its actual ADC and is able to accurately reflect the degree of water molecular motion. However, the image quality will reduce quickly and even the image will lose diagnostic value because the SNR and liver anatomy manifestation of the image will reduce quickly, and the artifact will increase at the same time as the b-value increases [22, 23]. Referring to this, Vossen [26] et al. demonstrated that image signals increased significantly while ADC values changed insignificantly if the technologies of parallel imaging or diffusion tensor imaging along with routine diffusion-weighted imaging were combined. From our experience, it is suitable to combine a small b-value with a large *b*-value in diffusion-weighted imaging scanning.

The immunohistochemistry specimens showed that this group of VX-2 tumor expression of the PCNA model was higher than peritumoral normal liver tissue ($p < 0.01$), and peritumoral tissue was higher than the tumor center and normal liver tissue; the researchers [27, 28] showed that PCNA is a cell proliferation antigen, reflecting the activity of cell proliferation, and histopathological grading was significantly positively related to the invasive potential of the cells and strength of the type of liver cancer associated with PCNA. Although the stronger differentiation is worse in tumor cells, PCNA expression in this experiment and the correlation analysis revealed that the tumor ADC value and PCNA expression were negatively correlated ($p < 0.01$). It can be considered that the expression of cell proliferation-related genes indicates the capability of tumor proliferation, so the water molecules in the tumor were internal diffusion limited, and the ADC values decreased.

What has been discussed above shows that the ADC is able to reflect not only water diffusion motion of VX-2 tumors, but also the generatation and death of tumor cells.

The ADC is affected by the *b*-value and microcirculation blood flow, etc. The ADC of the tumor measured dynamically and quantitatively is valuable to help understand the histological characteristics, monitor tumor growth and evaluate the degree of malignancy and therapeutic effect.

Acknowledgments Supported by the National Natural Science Foundation of China (no. 30070235, 30470508), Hunan Natural Science Foundation (no. 07JJ4022), Hunan Province Science and Technology Foundation (no. 06FJ3120, 07SK3072, 10SK3066, 10TD2030) and Changsha City Science and Technology Foundation (no. K1005023-31).

References

1. Lewin M, Arrivé L, Lacombe C, Vignaud A, Azizi L, Raynal M, et al. Diffusion-weighted MR imaging of liver pathology: principles and clinical applications. J Radiol. 2010;91(1 Pt1):11–26.
2. Bonekamp S, Jolepalem P, Lazo M, Gulsun MA, Kiraly AP, Kamel IR. Hepatocellular carcinoma: response to TACE assessed with semiautomated volumetric and functional analysis of diffusion-weighted and contrast-enhanced MR imaging data. Radiology. 2011;260(3):752–61.
3. Yang DM, Jahng GH, Kim HC, Jin W, Ryu CW, Nam DH, et al. The detection and discrimination of malignant and benign focal hepatic lesions: T2 weighted vs diffusion-weighted MRI. Br J Radiol. 2011;84(1000):319–26.
4. Nishie A, Tajima T, Asayama Y, Ishigami K, Kakihara D, Nakayama T, et al. Diagnostic performance of apparent diffusion coefficient for predicting histological grade of hepatocellular carcinoma. Eur J Radiol. 2011;80(2):e29–33.
5. Shiehmorteza M, Sirlin CB, Wolfson T, Gamst A, Soumekh AE, Heaton SP, et al. Effect of shot number on the calculated apparent diffusion coefficient in phantoms and in human liver in diffusion-weighted echo-planar imaging. J Magn Reson Imaging. 2009; 30(3):547–53.
6. Kim JE, Kim SH, Lee SJ, Rhim H. Hypervascular hepatocellular carcinoma 1 cm or smaller in patients with chronic liver disease: characterization with gadoxetic acid-enhanced MRI that includes diffusion-weighted imaging. Am J Roentgenol. 2011;196(6): W758–65.
7. Yu JS, Chung JJ, Kim JH, Cho ES, Kim DJ, Ahn JH, et al. Detection of small intrahepatic metastases of hepatocellular carcinomas using diffusion-weighted imaging: comparison with conventional dynamic MRI. Magn Reson Imaging. 2011;29(7): 985–92.
8. Kim YK, Kim CS, Han YM, Lee YH. Detection of liver malignancy with gadoxetic acid-enhanced MRI: is addition of diffusion-weighted MRI beneficial? Clin Radiol. 2011;66(6): 489–96.
9. Piana G, Trinquart L, Meskine N, Barrau V, Beers BV, Vilgrain V. New MR imaging criteria with a diffusion-weighted sequence for the diagnosis of hepatocellular carcinoma in chronic liver diseases. J Hepatol. 2011;55(1):126–32.
10. Saito K, Araki Y, Park J, Metoki R, Katsuyama H, Nishio R, et al. Effect of Gd-EOB-DTPA on T2-weighted and diffusion-weighted images for the diagnosis of hepatocellular carcinoma. J Magn Reson Imaging. 2010;32(1):229–34.
11. Koike N, Cho A, Nasu K, Seto K, Nagaya S, Ohshima Y, et al. Role of diffusion-weighted magnetic resonance imaging in the differential diagnosis of focal hepatic lesions. World J Gastroenterol. 2009;15(46):5805–12.
12. Miller FH, Hammond N, Siddiqi AJ, Shroff S, Khatri G, Wang Y, et al. Utility of diffusion-weighted MRI in distinguishing benign and malignant hepatic lesions. J Magn Reson Imaging. 2010; 32(1):138–47.
13. Heo SH, Jeong YY, Shin SS, Kim JW, Lim HS, Lee JH, et al. Apparent diffusion coefficient value of diffusion-weighted imaging for hepatocellular carcinoma: correlation with the histologic differentiation and the expression of vascular endothelial growth factor. Korean J Radiol. 2010;11(3):295–303.
14. Liu YB, Liang CH, Wang QS, Xie SF, Yu YX, Zhang ZL, et al. Clinical study of transcatheter arterial chemoembolization plus radiofrequency ablation in hepatocellular carcinoma by magnetic resonance imaging and functional diffusion-weighted imaging. Zhonghua Yi Xue Za Zhi. 2010;90(41):2922–6.
15. Mannelli L, Kim S, Hajdu CH, Babb JS, Clark TW, Taouli B, et al. Assessment of tumor necrosis of hepatocellular carcinoma after chemoembolization: diffusion-weighted and contrast-enhanced MRI with histopathologic correlation of the explanted liver. Am J Roentgenol. 2009;193(4):1044–52.
16. Muhi A, Ichikawa T, Motosugi U, Sano K, Matsuda M, Kitamura T, et al. High-*b*-value diffusion-weighted MR imaging of hepatocellular lesions: estimation of grade of malignancy of hepatocellular carcinoma. J Magn Reson Imaging. 2009;30(5): 1005–11.
17. Kim SY, Lee SS, Byun JH, Park SH, Kim JK, Park B, et al. Malignant hepatic tumors: short-term reproducibility of apparent diffusion coefficients with breath-hold and respiratory-triggered diffusion-weighted MR imaging. Radiology. 2010;255(3): 815–23.
18. Yuan YH, Xiao E-H, Liu J-B, He Z, Jin K, Ma C, et al. Characteristics and pathological mechanism on magnetic resonance diffusion-weighted imaging after chemoembolization in rabbit liver VX-2 tumor model. World J Gastroenterol. 2007;13(43): 5699–706.
19. Yuan YH, Xiao E-H, Liu J-B, Tang KL, Jin K, Yi SJ, et al. MR diffusion-weighted imaging of rabbit liver VX-2 tumor. World J Gastroenterol. 2005;11(20):3070–4.
20. Yuan YH, Xiao E-H, Liu J-B, Tang KL, Jin K, Yi SJ, et al. Gene expression and MR diffusion-weighted imaging after chemoembolization in rabbit liver VX-2 tumor model. World J Gastroenterol. 2008;14(36):5557–63.
21. Yuan YH, Xiao E-H, Liu J-B, He Z, Jin K, Ma C, et al. Characteristics of liver on magnetic resonance diffusion-weighted imaging: dynamic and image pathological investigation in rabbit liver VX-2 tumor model. World J Gastroenterol. 2008;14(25): 3997–4004.
22. Wang JP, Bai RJ, Sun HR, Zhao X, Li YJ, Yang J, et al. Correlation between MR diffusion weighted imaging with malignant degree of rabbit liver VX2 tumor models. Zhonghua Yi Xue Za Zhi. 2009;89(31):2210–3.
23. Youn BJ, Chung JW, Son KR, Kim HC, Jae HJ, Lee JM, et al. Diffusion-weighted MR: therapeutic evaluation after chemoembolization of VX-2 carcinoma implanted in rabbit liver. Acad Radiol. 2008;15(5):593–600.
24. Deng J, Virmani S, Young J, Harris K, Yang GY, Rademaker A, et al. Diffusion-weighted PROPELLER MRI for quantitative assessment of liver tumor necrotic fraction and viable tumor volume in VX2 rabbits. J Magn Reson Imaging. 2008;27(5): 1069–76.
25. Deng J, Rhee TK, Sato KT, Salem R, Haines K, Paunesku T, et al. In vivo diffusion-weighted imaging of liver tumor necrosis in the VX2 rabbit model at 1.5 Tesla. Invest Radiol. 2006;41(4): 410–4.
26. Vossen JA, Buijs M, Geschwind JF, Liapi E, Prieto Ventura V, et al. Diffusion-weighted and Gd-EOB-DTPA-contrast-enhanced magnetic resonance imaging for characterization of tumor

necrosis in an animal model. J Comput Assist Tomogr. 2009; 33(4):626–30.
27. Shen SQ, Li K, et al. Expression and clinical significance of NET-1 and PCNA in hepatocellular carcinoma. Med Oncol (Northwood, London, England). 2008;25(3):341–5.
28. Muhi A, Ichikawa T, et al. High-b-value diffusion-weighted MR imaging of hepatocellular lesions: estimation of grade of malignancy of hepatocellular carcinoma. J Mag Reson Imaging JMRI. 2009;30(5):1005–11.